Available online at www.sciencedirect.com
ScienceDirect
Computers and Structures 86 (2008) 1594–1603
Computers & Structures
www.elsevier.com/locate/compstruc

Cylindrical bending of piezoelectric laminates with a higher order shear and normal deformation theory

Tarun Kant *, S.M. Shiyekar

Department of Civil Engineering, Indian Institute of Technology Bombay, Powai, Mumbai 400 076, India

Received 30 July 2007; accepted 17 January 2008
Available online 5 March 2008

Abstract

An analytical solution, based on a higher order shear and normal deformation theory, is presented for the cylindrical flexure of piezoelectric plates. The primary displacement terms are expanded in thickness coordinate and an exact nature of electric potential is obtained in actuator and sensing layers. The electric potential function is evaluated by solving a second order ordinary differential equation satisfying electric boundary conditions along thickness direction of piezoelectric layer. A unidirectional composite plate attached with distributed actuator and sensor layers is analyzed under electrical and mechanical loading conditions and comparison of results with exact solution is presented. Results for non-piezoelectric plates are also compared with elasticity and other solutions of cylindrical bending.

Keywords: Higher order theories; Piezoelectric plates; Cylindrical bending; Plane strain

1. Introduction

Materials with property to change shape and size when electrically charged and the reversal behavior is utilized in the controlling mechanism of the structures. Piezoelectric layers are embedded or attached to the elastic layers in patches or in a distributed form. Such structures are called as smart/intelligent or adaptive structures.

Tiersten [1] defined material constitutive relations of linear piezoelectricity. The equations of linear piezoelectricity are coupled with the charge equation of electrostatics by means of piezoelectric constants. Earlier Mindlin [2] presented approximate theory for the vibrations of piezoelectric plates.

Ray et al. [3] developed exact solutions for a mono-layered piezoelectric polymer polyvinyledene fluoride (PVDF) plate, under electric potential and mechanical loading. Numerical results are evaluated for thick and thin single piezoelectric layer. Ray et al. [4] further established elasticity solutions for smart unidirectional composite plates under cylindrical bending. Heyliger and Brooks [5] also presented exact solutions of plates with two different layers of piezoceramics, two layers of angle-ply piezopolymers and three layers of cross ply piezopolymers under cylindrical bending. Later Saravanos and Heyliger [6] presented a classified review of the analytical solutions presented by various investigators in the mechanics of the laminated piezoelectric structures. Exact plane strain solution for a piezoelectric orthotropic flat panel under mechanical, thermal, and electric loading is obtained by Dube et al. [7]. Shang et al. [8] also obtained exact plane strain solution for piezoelectric layers under thermal excitation. Dumir et al. [9] presented first order Reissner and Mindlin [10,11] plate (FOST) and classical Kirchhoff plate (CPT) solutions for hybrid plates in cylindrical bending under thermoelectric loading. Vel and Batra [12] used Eshelby–Stroh formulation to analyze cylindrical bending of laminated composite plate with segmented actuators and sensors for different boundary conditions under dynamic state. Static and dynamic response of adaptive angle-ply

* Corresponding author. Tel.: +91 22 2576 7310; fax: +91 22 2576 7302.
E-mail address: tkant@civil.iitb.ac.in (T. Kant).

0045-7949/$ - see front matter © 2008 Elsevier Ltd. All rights reserved.
doi:10.1016/j.compstruc.2008.01.002

laminates in cylindrical bending is studied by Chen et al. [13] using state space approach. Saravanos [14] discussed finite element (FE) formulation based on mixed theory. In this theory, elastic displacements are modeled by equivalent single layer (ESL) theory and electric potential is by layerwise (LW) approach. Similar approach is proposed by Ballhause et al. [15] who have presented statics and dynamics of piezoelectric plates. Piezoelectric plate elements based on Reissner–Mindlin assumptions is presented by Kogl and Bucalem [16] and Carrera [17]. Mannini and Gaudenzi [18] investigated a stress concentration problem in the smart composite using higher order FE model. An iterative FE solution is presented by Gaudenzi and Bathe [19] and is applied in the linear analysis of piezoelectric beam and non-linear analysis of an aluminum cantilever beam attached with piezoceramics. Roccella and Gaudenzi [20] used quadratic variation of electric potential through the thickness suggested by [19] in the formulation of piezoelectric plate model. Gaudenzi [21] developed a higher order beam model and also discussed the edge effect at the free boundary of the adaptive structure.

In this paper, a higher order shear and normal deformation theory (HOST8) is developed for the analytical solution of piezoelectric plates under plane strain condition. Eight degrees of freedom are used to expand primary displacement field whereas exact variation of electric field is obtained in the piezoelectric layers by solving the governing second order ordinary differential equation satisfying electrical boundary conditions in the thickness direction. Results are compared with exact solutions [4]. Kant [22], Manjunatha and Kant [23,24], Kant and Swaminathan [25], have contributed extensively to the development of higher order shear and normal deformation theories. Recently, Kant et al. [26] developed a novel semi-analytical methodology using mixed variables, by maintaining the fundamental elasticity relations between stress, strain and displacements. The method satisfies the requirements of the through thickness continuity of transverse stresses and displacements. Results are presented for laminates simply supported on all edges and under cylindrical bending. Kant et al. [27–29] also presented a new partial discretization mixed FE formulation for general laminates with any boundary conditions. Present results for non-piezoelectric plates under plane strain condition are compared with the elasticity [35], semi-analytical [26,30], partial FE [27–30] and Reissner and Mindlin [10,11] (FOST) solutions.

2. Coupled plane strain formulation

2.1. Displacement model

A rectangular smart plate structure is shown in Fig. 1. The length of the plate is denoted by a along x direction and y side is infinite. The geometrical configuration of the plate is such that the thickness dimension is along z direction. The top and bottom layers of the plate are of piezoelectric materials, which act as distributed actuator and sensor. The core of the plate called, substrate, is purely elastic and has any number of elastic layers.

Displacement components $u(x,z)$ and $w(x,z)$ at any point in the plate are expanded in a Taylor's series to approximate the two- dimensional (2D) elasticity problem as a one-dimensional (1D) plate problem in cylindrical bending. The assumed displacement fields are as follows:

Model: HOST8

$$\begin{aligned} u(x,z) &= u_0(x) + z\theta_x(x) + z^2 u_0^*(x) + z^3\theta_x^*(x) \\ w(x,z) &= w_0(x) + z\theta_z(x) + z^2 w_0^*(x) + z^3\theta_z^*(x) \end{aligned} \tag{1}$$

Model: FOST

$$\begin{aligned} u(x,z) &= u_0(x) + z\theta_x(x) \\ w(x,z) &= w_0(x) \end{aligned} \tag{2}$$

The following strain vector $[\varepsilon]$ is given by strain displacement relationship as per classical theory of elasticity:

$$\begin{Bmatrix} \varepsilon_x \\ \varepsilon_y \\ \varepsilon_z \\ \gamma_{xy} \\ \gamma_{yz} \\ \gamma_{xz} \end{Bmatrix} = \left\{ \frac{\partial u}{\partial x} \quad \frac{\partial v}{\partial y} \quad \frac{\partial w}{\partial z} \quad \frac{\partial u}{\partial y} + \frac{\partial v}{\partial x} \quad \frac{\partial v}{\partial z} + \frac{\partial w}{\partial y} \quad \frac{\partial u}{\partial z} + \frac{\partial w}{\partial x} \right\}^t \tag{3}$$

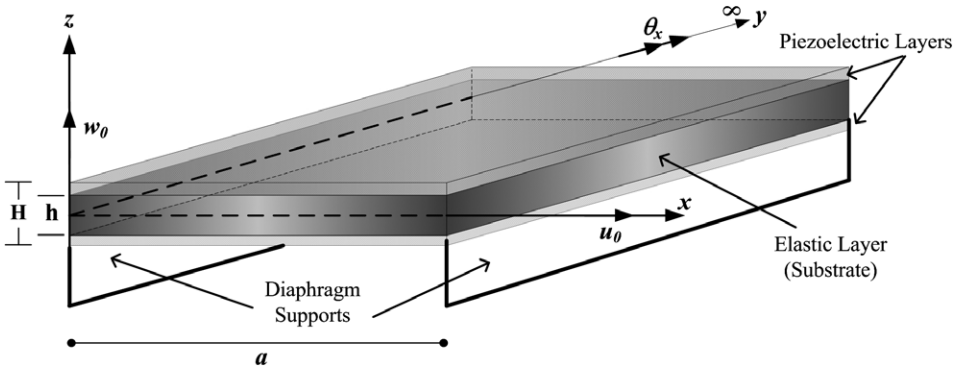

Fig. 1. Geometry of piezoelectric plate simply (diaphragm) supported on two infinite opposite edges and positive set of displacement components.

2.2. Constitutive equations

The linear constitutive relations for a single piezoelectric layer couples the elastic and electric fields as given below [1].

$$\{\sigma\} = [C]\{\varepsilon\} - [e]\{E\}$$
$$\{D\} = [e]^t\{\varepsilon\} + [g]\{E\} \tag{4}$$

Eq. (4) can be further expanded for ith layer of the plate as

$$\begin{Bmatrix}\sigma_1\\ \sigma_2\\ \sigma_3\\ \tau_{12}\\ \tau_{23}\\ \tau_{13}\end{Bmatrix} = \begin{bmatrix} C_{11} & C_{12} & C_{13} & 0 & 0 & 0\\ C_{12} & C_{22} & C_{23} & 0 & 0 & 0\\ C_{13} & C_{23} & C_{33} & 0 & 0 & 0\\ 0 & 0 & 0 & C_{44} & 0 & 0\\ 0 & 0 & 0 & 0 & C_{55} & 0\\ 0 & 0 & 0 & 0 & 0 & C_{66}\end{bmatrix}\begin{Bmatrix}\varepsilon_1\\ \varepsilon_2\\ \varepsilon_3\\ \gamma_{12}\\ \gamma_{23}\\ \gamma_{13}\end{Bmatrix} - \begin{bmatrix} 0 & 0 & e_{31}\\ 0 & 0 & e_{32}\\ 0 & 0 & e_{33}\\ 0 & 0 & 0\\ 0 & e_{24} & 0\\ e_{15} & 0 & 0\end{bmatrix}\begin{Bmatrix}E_1\\ E_2\\ E_3\end{Bmatrix}$$

$$\begin{Bmatrix}D_1\\ D_2\\ D_3\end{Bmatrix} = \begin{bmatrix} 0 & 0 & e_{31}\\ 0 & 0 & e_{32}\\ 0 & 0 & e_{33}\\ 0 & 0 & 0\\ 0 & e_{24} & 0\\ e_{15} & 0 & 0\end{bmatrix}^t\begin{Bmatrix}\varepsilon_1\\ \varepsilon_2\\ \varepsilon_3\\ \gamma_{12}\\ \gamma_{23}\\ \gamma_{13}\end{Bmatrix} + \begin{bmatrix} g_{11} & 0 & 0\\ 0 & g_{22} & 0\\ 0 & 0 & g_{33}\end{bmatrix}\begin{Bmatrix}E_1\\ E_2\\ E_3\end{Bmatrix} \tag{5}$$

where $\sigma, C, \varepsilon, e, E, D$ and g are, stress vector, elastic constant matrix, strain vector, piezoelectric constant matrix, electric field intensity vector, electric displacement vector and dielectric constant matrix. The elastic constants are expressed in terms of material constants as

$$C_{11} = \frac{E_1(1-\nu_{23}\nu_{32})}{\Delta}, \quad C_{22} = \frac{E_2(1-\nu_{13}\nu_{31})}{\Delta}, \quad C_{44} = G_{12}$$
$$C_{12} = \frac{E_1(\nu_{21}+\nu_{31}\nu_{23})}{\Delta}, \quad C_{23} = \frac{E_2(\nu_{32}+\nu_{12}\nu_{31})}{\Delta}, \quad C_{55} = G_{23}$$
$$C_{13} = \frac{E_1(\nu_{31}+\nu_{21}\nu_{32})}{\Delta}, \quad C_{33} = \frac{E_3(1-\nu_{12}\nu_{21})}{\Delta}, \quad C_{66} = G_{13}$$
$$\Delta = (1-\nu_{12}\nu_{21}-\nu_{23}\nu_{32}-\nu_{31}\nu_{13}-2\nu_{12}\nu_{23}\nu_{31})$$

The electric field intensity vector E is related to electrostatic potential ξ in the Lth layer as

$$E_x^L = -\frac{\partial\xi^L}{\partial x}, \quad E_y^L = -\frac{\partial\xi^L}{\partial y}, \quad E_z^L = -\frac{\partial\xi^L}{\partial z} \tag{6}$$

The piezoelectric constant matrix $[e]$ and the dielectric matrix $[g]$ for polyvinyledene fluoride (PVDF) commonly known as PVDF polymer are given in [31,32] and the Maxwell's charge equilibrium equation [33] can be written as

$$\frac{\partial D_x}{\partial x} + \frac{\partial D_y}{\partial y} + \frac{\partial D_z}{\partial z} = 0 \tag{7}$$

Considering the problem as a plane strain problem, strain quantities in y direction are zero ($\varepsilon_y = \gamma_{xy} = \gamma_{yz} = 0$). The strain displacement relationship of Eq. (3) becomes

$$\varepsilon_x = \frac{\partial u}{\partial x}, \quad \varepsilon_z = \frac{\partial w}{\partial z}, \quad \gamma_{xz} = \frac{\partial u}{\partial z} + \frac{\partial w}{\partial x} \tag{8}$$

Eqs. (9) and (10) show the expansion of elastic (e) and piezoelectric (pz) stress vectors

$$\begin{Bmatrix}\sigma_x\\ \sigma_z\\ \tau_{xz}\end{Bmatrix}^e = \begin{bmatrix} C_{11} & C_{12} & 0\\ C_{12} & C_{22} & 0\\ 0 & 0 & C_{33}\end{bmatrix}\begin{Bmatrix}\varepsilon_x\\ \varepsilon_z\\ \gamma_{xz}\end{Bmatrix} \tag{9}$$

$$C_{11} = \frac{E_1(1-\nu_{23}\nu_{32})}{\Delta}, \quad C_{22} = \frac{E_3(1-\nu_{12}\nu_{21})}{\Delta}$$
$$C_{12} = C_{21} = \frac{E_1(\nu_{31}+\nu_{21}\nu_{32})}{\Delta}, \quad C_{33} = G_{13}$$
$$\Delta = (1-\nu_{12}\nu_{21}-\nu_{13}\nu_{31}-\nu_{23}\nu_{32}-2\nu_{12}\nu_{31}\nu_{23})$$
$$\sigma_x^{pz} = e_{31}\left(-\frac{\partial\xi}{\partial z}\right), \quad \sigma_z^{pz} = e_{33}\left(-\frac{\partial\xi}{\partial z}\right),$$
$$\tau_{xz}^{pz} = e_{15}\left(-\frac{\partial\xi}{\partial x}\right). \tag{10}$$

where C_{ij} are elastic constants corresponding to plane strain state in x–z plane.

The electric displacement vector (D) is also expanded in the following equations with $D_y = 0$ as:

$$D_x = e_{15}\left(\frac{\partial u}{\partial z} + \frac{\partial w}{\partial x}\right) + g_{11}\left(-\frac{\partial\xi}{\partial x}\right)$$
$$D_z = e_{31}\left(\frac{\partial u}{\partial x}\right) + e_{33}\left(\frac{\partial w}{\partial z}\right) + g_{33}\left(-\frac{\partial\xi}{\partial z}\right) \tag{11}$$

2.3. Governing equations of equilibrium

The equations of equilibrium are derived by using the principle of minimum potential energy. In analytical form it can be written as

$$\delta(U+V) = 0 \tag{12}$$

where U is the total strain energy due to deformation, V is the potential of the external loads and $U+V=\pi$ is the total potential energy and δ is the variational symbol. Substituting the appropriate energy expressions in the above equation, the final expression can be written as

$$\left[\int_{-h/2}^{+h/2}\int_l (\sigma_x\delta\varepsilon_x + \sigma_z\delta\varepsilon_z + \tau_{xz}\delta\gamma_{xz})\mathrm{d}x\,\mathrm{d}z - \int_l q_0^+\delta w^+\mathrm{d}x\right] = 0 \tag{13}$$

where $w^+ = w_0 + (h/2)\theta_z + (h^2/4)w_0^* + (h^3/8)\theta_z^*$ is the transverse displacement at top surface of the plate. q_0^+ is

the transverse load applied at top of the plate. Integrating Eq. (13) by parts and collecting the coefficients of $\delta u_0, \delta w_0, \delta\theta_x, \delta\theta_z, \delta u_0^*, \delta w_0^*, \delta\theta_x^*, \delta\theta_z^*$, the following equations of equilibrium are obtained:

$$\begin{aligned}
&\delta u_0 : \frac{\partial N_x}{\partial x} = 0, \quad \delta\theta_x^* : \frac{\partial M_x^*}{\partial x} - 3Q_x^* = 0\\
&\delta w_0 : \frac{\partial Q_x}{\partial x} + q_0^+ = 0, \quad \delta u_0^* : \frac{\partial N_x^*}{\partial x} - 2S_x = 0\\
&\delta\theta_x : \frac{\partial M_x}{\partial x} - Q_x = 0, \quad \delta w_0^* : \frac{\partial Q_x^*}{\partial x} - 2M_z^* + \left(\frac{h^2}{4}\right)q_0^+ = 0\\
&\delta\theta_z : \frac{\partial S_x}{\partial x} - N_z + \left(\frac{h}{2}\right)q_0^+ = 0\\
&\delta\theta_z^* : \frac{\partial S_x^*}{\partial x} - 3N_z^* + \left(\frac{h^3}{8}\right)q_0^+ = 0
\end{aligned} \tag{14}$$

The two components of stress resultants, in terms of elastic and piezoelectric stress components, are defined by

$$\begin{aligned}
&M_x^e = \sum_{L=1}^{n}\int_{Z_L}^{Z_{L+1}} \sigma_x^e z\,dz, \quad M_x^{pz} = \sum_{L=1}^{n}\int_{Z_L}^{Z_{L+1}} \sigma_x^{pz} z\,dz\\
&M_x^{e^*} = \sum_{L=1}^{n}\int_{Z_L}^{Z_{L+1}} \sigma_x^e z^3\,dz, \quad M_x^{pz^*} = \sum_{L=1}^{n}\int_{Z_L}^{Z_{L+1}} \sigma_x^{pz} z^3\,dz\\
&M_z^e = \sum_{L=1}^{n}\int_{Z_L}^{Z_{L+1}} \sigma_z^e z\,dz, \quad M_z^{pz} = \sum_{L=1}^{n}\int_{Z_L}^{Z_{L+1}} \sigma_z^{pz} z\,dz\\
&Q_x^e = \sum_{L=1}^{n}\int_{Z_L}^{Z_{L+1}} \tau_{xz}^e\,dz, \quad Q_x^{pz} = \sum_{L=1}^{n}\int_{Z_L}^{Z_{L+1}} \tau_{xz}^{pz}\,dz\\
&Q_x^{e^*} = \sum_{L=1}^{n}\int_{Z_L}^{Z_{L+1}} \tau_{xz}^e z^2\,dz, \quad Q_x^{pz^*} = \sum_{L=1}^{n}\int_{Z_L}^{Z_{L+1}} \tau_{xz}^{pz} z^2\,dz\\
&S_x^e = \sum_{L=1}^{n}\int_{Z_L}^{Z_{L+1}} \tau_{xz}^e z\,dz, \quad S_x^{pz} = \sum_{L=1}^{n}\int_{Z_L}^{Z_{L+1}} \tau_{xz}^{pz} z\,dz\\
&S_x^{e^*} = \sum_{L=1}^{n}\int_{Z_L}^{Z_{L+1}} \tau_{xz}^e z^3\,dz, \quad S_x^{pz^*} = \sum_{L=1}^{n}\int_{Z_L}^{Z_{L+1}} \tau_{xz}^{pz} z^3\,dz\\
&N_x^e = \sum_{L=1}^{n}\int_{Z_L}^{Z_{L+1}} \sigma_x^e\,dz, \quad N_x^{pz} = \sum_{L=1}^{n}\int_{Z_L}^{Z_{L+1}} \sigma_x^{pz}\,dz\\
&N_x^{e^*} = \sum_{L=1}^{n}\int_{Z_L}^{Z_{L+1}} \sigma_x^e z^2\,dz, \quad N_x^{pz^*} = \sum_{L=1}^{n}\int_{Z_L}^{Z_{L+1}} \sigma_x^{pz} z^2\,dz\\
&N_z^e = \sum_{L=1}^{n}\int_{Z_L}^{Z_{L+1}} \sigma_z^e\,dz, \quad N_z^{pz} = \sum_{L=1}^{n}\int_{Z_L}^{Z_{L+1}} \sigma_z^{pz}\,dz\\
&N_z^{e^*} = \sum_{L=1}^{n}\int_{Z_L}^{Z_{L+1}} \sigma_z^e z^2\,dz, \quad N_z^{pz^*} = \sum_{L=1}^{n}\int_{Z_L}^{Z_{L+1}} \sigma_z^{pz} z^2\,dz
\end{aligned} \tag{15}$$

$$\begin{aligned}
&M_x = M_x^e + M_x^{pz}, \quad N_x^* = N_x^{e^*} + N_x^{pz^*}\\
&M_z = M_z^e + M_z^{pz}, \quad S_x = S_x^e + S_x^{pz}\\
&M_x^* = M_x^{e^*} + M_x^{pz^*}, \quad S_x^* = S_x^{e^*} + S_x^{pz^*}\\
&Q_x = Q_x^e + Q_x^{pz}, \quad N_z = N_z^e + N_z^{pz}\\
&Q_x^* = Q_x^{e^*} + Q_x^{pz^*}, \quad N_z^* = N_z^{e^*} + N_z^{pz^*}\\
&N_x = N_x^e + N_x^{pz}
\end{aligned} \tag{16}$$

Eq. (16) defines the total stress resultants, i.e. the addition of elastic and piezoelectric stress resultants. It is to be noted that both elastic and piezoelectric fields are indeed coupled through the constitutive relations (Eq. (4)) and this automatically gives rise to definition of elastic and piezoelectric stress resultants given above by Eq. (15).

3. Analytical solution

Following are the boundary conditions used for two opposite infinite length simply (diaphragm) supported edges

$$\begin{aligned}
\text{At edges } x = 0 \quad \text{and} \quad x = a : w_0 = 0, \quad \theta_z = 0,\\
M_x = 0, \quad N_x = 0, \quad w_0^* = 0, \quad \theta_z^* = 0,\\
M_x^* = 0, \quad N_x^* = 0
\end{aligned}$$

Navier's solution procedure is adopted to compute displacement variables. Displacements, which satisfy the above boundary conditions exactly, can be assumed as follows:

$$\begin{aligned}
&u_0 = \sum_{m=1}^{\infty} u_{0_m}\cos\left(\frac{m\pi x}{a}\right), \quad u_0^* = \sum_{m=1}^{\infty} u_{0_m}^*\cos\left(\frac{m\pi x}{a}\right)\\
&w_0 = \sum_{m=1}^{\infty} w_{0_m}\sin\left(\frac{m\pi x}{a}\right), \quad w_0^* = \sum_{m=1}^{\infty} w_{0_m}^*\sin\left(\frac{m\pi x}{a}\right)\\
&\theta_x = \sum_{m=1}^{\infty} \theta_{x_m}\cos\left(\frac{m\pi x}{a}\right), \quad \theta_x^* = \sum_{m=1}^{\infty} \theta_{x_m}^*\cos\left(\frac{m\pi x}{a}\right)\\
&\theta_z = \sum_{m=1}^{\infty} \theta_{z_m}\sin\left(\frac{m\pi x}{a}\right), \quad \theta_z^* = \sum_{m=1}^{\infty} \theta_{z_m}^*\sin\left(\frac{m\pi x}{a}\right)\\
&q_z^+ = \sum_{m=1}^{\infty} q_{0_m}^+\sin\left(\frac{m\pi x}{a}\right), \quad \xi(x,z) = \sum_{m=1}^{\infty} \xi_m(z)\sin\left(\frac{m\pi x}{a}\right)
\end{aligned} \tag{17}$$

The procedure to obtain through thickness electric potential $\xi_m(z)$ is explained in the following section.

3.1. Electrostatic potential

The constitutive relationship between elastic and electric fields is expressed in Eq. (4) and the relationship between electric field intensity vector E and electrostatic potential ξ is stated in Eq. (6). Substituting Eq. (6) in second of Eq. (4), and expanding electric displacement vector D in x, y and z directions, Eq. (11) is obtained, which represents the relationship between electric displacements, electrostatic potential and elastic strains.

The elastic strains are already described for plane strain state in Eq. (8). Thus the final form of Eq. (11) will contain higher order terms of elastic displacements.

Following second order ordinary differential equation (ODE) is obtained by substituting the final form of Eq. (11) in 3D charge equilibrium equation given by Eq. (7)

$$\eta_m\xi_m''(z) - \lambda_m\xi_m(z) + \Psi_m = 0 \tag{18}$$

where the coefficients of above ODE are

$$\eta_m = a^2 g_{33}$$
$$\lambda_m = \pi^2 g_{11}$$
$$\Psi_m = a(e_{31}\pi(\theta_{x_m} + 2z u^*_{0_m} + 3z^2\theta^*_{x_m}))$$

The above coefficients are in terms of higher order elastic displacements and the closed form solution of the above ODE is obtained by applying electric boundary conditions along z direction for actuator and sensor as:

Actuator function: Applying two through thickness electric boundary conditions for actuator layer, first at top interface between substrate and piezoelectric layer, electric potential is zero ($z = h/2$, $\xi_m = 0$) and second is, at top of the smart plate, there is a prescribed amplitude of electric potential ($z = H/2$, $\xi_m = V_t$), where H is the total thickness of plate and h is thickness of the substrate.

The solution of actuator function is obtained as follows:

$$\xi^a_m(z) = \frac{-\left(4\left(\psi_m \cosh\left[\frac{(2H-h-2z)\sqrt{\lambda_m}}{4\sqrt{\eta_m}}\right] + (V_t\lambda_m - \psi_m)\cosh\left[\frac{(h-2z)\sqrt{\lambda_m}}{4\sqrt{\eta_m}}\right]\right)\left(\cosh\left[\frac{(H+h)\sqrt{\lambda_m}}{2\sqrt{\eta_m}}\right] + \sinh\left[\frac{(H+h)\sqrt{\lambda_m}}{2\sqrt{\eta_m}}\right]\right)\sinh\left[\frac{(h-2z)\sqrt{\lambda_m}}{4\sqrt{\eta_m}}\right]\right)}{\lambda_m\left(\cosh\left[\frac{H\sqrt{\lambda_m}}{\sqrt{\eta_m}}\right] - \cosh\left[\frac{h\sqrt{\lambda_m}}{\sqrt{\eta_m}}\right] + \sinh\left[\frac{H\sqrt{\lambda_m}}{\sqrt{\eta_m}}\right] - \sinh\left[\frac{h\sqrt{\lambda_m}}{\sqrt{\eta_m}}\right]\right)} \tag{19}$$

Sensor function: Similarly applying two through thickness electric boundary conditions for sensor layer, first at bottom interface, electric potential is zero ($z = -h/2$, $\xi_m = 0$) as Dirichlet boundary condition. The second boundary condition is prescribed at bottom of smart plate, i.e. electric displacement is zero ($z = -H/2$, $D_z = 0$), as Neumann boundary condition. Using above mixed boundary conditions, the solution of sensor function is obtained as follows:

$$\xi^s_m(z) = \frac{-\left(4\left(\cosh\left[\frac{(H+h)\sqrt{\lambda_m}}{2\sqrt{\eta_m}}\right] + \sinh\left[\frac{(H+h)\sqrt{\lambda_m}}{2\sqrt{\eta_m}}\right]\right)\left(\Gamma_m\sqrt{\lambda_m}\cosh\left[\frac{(h+2z)\sqrt{\lambda_m}}{4\sqrt{\eta_m}}\right] + \sqrt{\eta_m}\psi_m \sinh\left[\frac{(2H-h+2z)\sqrt{\lambda_m}}{4\sqrt{\eta_m}}\right]\right)\sinh\left[\frac{(h+2z)\sqrt{\lambda_m}}{4\sqrt{\eta_m}}\right]\right)}{\sqrt{\eta_m}\lambda_m\left(\cosh\left[\frac{H\sqrt{\lambda_m}}{\sqrt{\eta_m}}\right] + \cosh\left[\frac{h\sqrt{\lambda_m}}{\sqrt{\eta_m}}\right] + \sinh\left[\frac{H\sqrt{\lambda_m}}{\sqrt{\eta_m}}\right] + \sinh\left[\frac{h\sqrt{\lambda_m}}{\sqrt{\eta_m}}\right]\right)} \tag{20}$$

where $\Gamma_m = e_{31}\pi(u_{0_m} + z(\theta_{x_m} + z(u^*_{0_m} + z\theta^*_{x_m})))$.

The electric boundary conditions show that the substrate layer is grounded.

Eqs. (19) and (20) give the exact, closed form solution for electrostatic potentials $\xi^a_m(z)$ and $\xi^s_m(z)$ for both actuator and sensor layers, respectively, in terms of higher order elastic displacements.

The above electrostatic potential satisfies all the boundary conditions, constitutive relationship, which couples the elastic and electric fields and 3D charge equilibrium equation and is thus free from any assumptions.

After the evaluation of electric potential functions, the piezoelectric stress vectors are calculated from Eq. (10) by substituting actuating electric function when voltage is applied. Finally, piezoelectric stress resultants are evaluated from second set of Eq. (15). Similarly elastic stress vectors and elastic stress resultants are calculated from Eq. (9) and first set of Eq. (15), respectively. Displacements are obtained by solving linear algebraic equations by substituting total stress resultants from Eq. (16) in equilibrium equations given by Eq. (14). Transverse shearing stress (τ_{xz}) and normal stress (σ_z) are evaluated by integrating the equilibrium equations of elasticity as per

$$\tau^L_{xz} = -\sum_{L=1}^{n}\int_{Z_{L-1}}^{Z_L}\left(\frac{\partial\sigma_x}{\partial x}\right)dz, \quad \sigma^L_z = -\sum_{L=1}^{n}\int_{Z_{L-1}}^{Z_L}\left(\frac{\partial\tau_{xz}}{\partial x}\right)dz$$

4. Numerical results

Results are presented for piezoelectric plate under cylindrical bending simply supported on two opposite infinite edges. The laminate or substrate is unidirectional layer of graphite/epoxy composite, where the piezoelectric material is of PVDF, attached at top and bottom of the unidirectional composite plate functioning as actuator and sensor.

The material properties for an elastic layer and PVDF are as follows.

Elastic layer [4]

$$E_L = 172.5 \times 10^9\ \mathrm{N/m^2}, \quad E_T = 6.9 \times 10^9\ \mathrm{N/m^2},$$
$$G_{LT} = 3.45 \times 10^9\ \mathrm{N/m^2}$$
$$v_{LT} = 0.25, \quad v_{TT} = 0.25$$

Table 1
Material properties for polyvinyledene fluoride/PVDF polymer

Property	PVDF
e_{31} (c/m^2)	0.0460
e_{15} (c/m^2)	0.0000
e_{33} (c/m^2)	0.0000
g_{11} (F/m)	0.1062×10^{-9}
g_{33} (F/m)	0.1062×10^{-9}
Poisson's ratio	0.2900
Modulus of elasticity (N/m^2)	2.0×10^9

L and T are directions parallel and perpendicular to fiber direction, respectively, and Table 1 shows the properties of PVDF material [34].

The thicknesses of the sensor and actuator layers are 40 μm. Considering $m = 1$, the numerical results are evaluated for

Case (i) : Singly sinusoidal mechanical load ($q_0 = 10$ N/m^2) without applied voltage at top of actuator ($V = 0$) and,

Case (ii) : Singly sinusoidal mechanical load ($q_0 = 10$ N/m^2) with applied voltage at top of actuator ($V = 100$).

The electrical boundary conditions are: at edges, $x = 0$ and a, electric potential are zero and also the laminate is not permitting any charge through the thickness, thus edges and core substrate are grounded.

The results are non-dimensionalized as

$$\bar{u}\left(0, \pm\frac{z}{H}\right) = \frac{100E_T}{q_0 S^4 H}(u), \quad \bar{w}\left(\frac{a}{2}, \pm\frac{z}{H}\right) = \frac{100E_T}{q_0 S^4 H}(w)$$

$$\bar{\sigma}_x\left(\frac{a}{2}, \pm\frac{z}{H}\right) = \frac{\sigma_x}{q_0 S^2}, \quad \bar{\sigma}_z\left(\frac{a}{2}, \pm\frac{z}{H}\right) = \frac{\sigma_z}{q_0}$$

$$\bar{\tau}_{xz}\left(0, \pm\frac{z}{H}\right) = \frac{\tau_{xz}}{q_0}$$

Results are compared with 3D exact solution [4] for piezoelectric plate. For non-piezoelectric plate of a unidirectional orthotropic plate (0^0) with fibers oriented in x direction, results are compared and normalized with elasticity solution [35]. Figs. 2a–2d show the results of displacements and stresses for an orthotropic laminate subjected to sinusoidal transverse mechanical load. Reissner and Mindlin [10,11] (FOST) theory is also parallely formulated to compare the results for non-piezoelectric unidirectional plate under transverse mechanical loading. Table 2 shows the comparison of present theory with elasticity, semi-analytical, partial FEM and FOST solutions.

Figs. 3a and 3b show normalized in-plane displacement (u) under case (i) and case (ii) for $a/H = 4$ and 10, respectively. The reversal bending of the elastic layer caused by actuator shows the opposite nature of the in-plane displacement. Variation of normalized transverse displacement (w) along the thickness of the thick plate ($a/H = 4$) is shown in Fig. 4a for both types of loading. Fig. 4b shows more electric potential is required for the reversal bending of thin plate ($a/H = 100$) and displacement of the thin plate

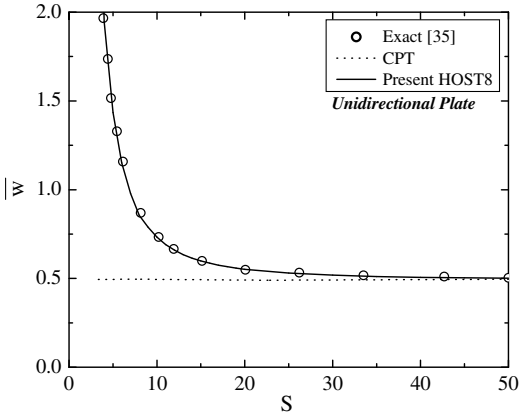

Fig. 2a. Comparison of central normalized variation of transverse displacement ($\bar{w}$) for various span to thickness ratios ($a/h = S$) for a unidirectional plate subjected to singly sinusoidal mechanical loading.

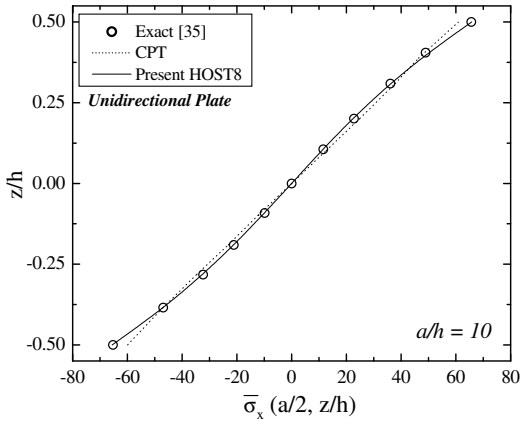

Fig. 2b. Comparison of central normalized variation of normal stress ($\bar{\sigma}_x$) for a unidirectional plate subjected to singly sinusoidal mechanical loading.

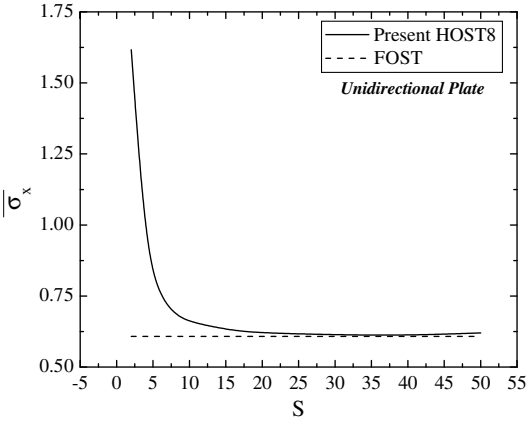

Fig. 2c. Comparison of normalized variation of top normal stress ($\bar{\sigma}_x$) for various span to length ratios ($a/h = S$) for a unidirectional plate subjected to singly sinusoidal mechanical loading.

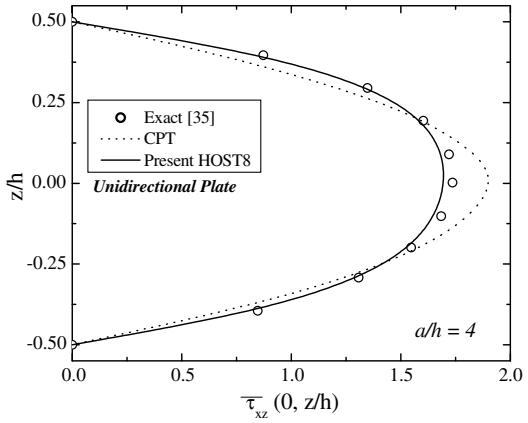

Fig. 2d. Comparison of normalized variation of transverse shear stress ($\bar{\tau}_{xz}$) for a unidirectional plate ($a/h = 4$) subjected to singly sinusoidal mechanical loading.

Table 2
Comparison with other plane strain solutions of non-piezoelectric unidirectional laminate subjected to transverse singly sinusoidal mechanical load

S	Source	σ_x ($a/2$, $h/2$)	σ_x ($a/2$, $-h/2$)	τ_{xz} (max)	w ($a/2$, 0)
4	Present HOST8	0.8920	−0.8497	0.4258	1.9443
		[−0.954]	[0.188]	[−1.662]	[−0.241]
	Semi-analytical[a]	0.9006	−0.8481	0.4328	1.9489
		[0.000]	[0.000]	[−0.046]	[−0.005]
	Partial FEM[a]	0.8204	−0.7710	0.4759	1.9906
		[8.844]	[−9.091]	[9.907]	[2.134]
	FOST[b]	0.6079	−0.6079	0.4774	1.756
		[−32.50]	[−28.32]	[10.254]	[−9.90]
	Elasticity[c]	0.9006	−0.8481	0.4330	1.9490
10	Present HOST8	0.6541	−0.6587	0.4679	0.7311
		[−0.728]	[0.549]	[−0.085]	[−0.109]
	Semi-analytical[a]	0.6569	−0.6551	0.4683	0.7319
		[0.000]	[0.000]	[0.000]	[0.000]
	Partial FEM[a]	0.6432	−0.6414	0.4788	0.7306
		[−2.085]	[−2.091]	[2.242]	[−0.177]
	FOST[b]	0.6079	−0.6079	0.4774	0.6921
		[−7.459]	[−7.205]	[1.943]	[−5.437]
	Elasticity[c]	0.6569	−0.6551	0.4683	0.7319
20	Present HOST8	0.6194	−0.6212	0.4750	0.5514
		[−0.145]	[0.161]	[−0.021]	[−0.09]
	Semi-analytical[a]	0.6203	−0.6202	0.4751	0.5519
		[0.000]	[0.000]	[0.000]	[0.000]
	Partial FEM[a]	0.6070	−0.6068	0.4820	0.5499
		[−2.144]	[−2.160]	[1.452]	[−0.362]
	FOST[b]	0.6079	−0.6079	0.4774	0.5401
		[−1.999]	[−1.983]	[0.484]	[−2.138]
	Elasticity[c]	0.6203	−0.6202	0.4751	0.5519
50	Present HOST8	0.6097	−0.6100	0.4770	0.5008
		[0.032]	[0.082]	[0.020]	[−0.07]
	Semi-analytical[a]	0.6095	−0.6095	0.4769	0.5012
		[0.000]	[0.000]	[0.000]	[0.000]
	Partial FEM[a]	0.600	−0.600	0.4847	0.5000
		[−1.558]	[−1.558]	[1.635]	[0.239]
	FOST[b]	0.6079	−0.6079	0.4774	0.4975
		[−0.262]	[−0.262]	[0.104]	[−0.738]
	Elasticity[c]	0.6095	−0.6095	0.4769	0.5012

[ ] % Error w.r.t elasticity solution.
[a] Pendhari [30].
[b] Reissner and Mindlin [10,11].
[c] Pagano [35].

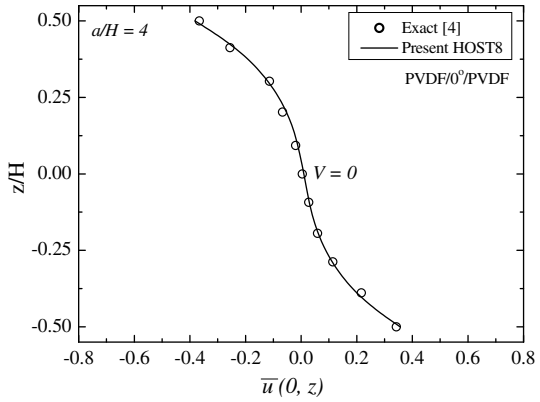

Fig. 3a. Comparison of normalized variation of in-plane displacement ($\bar{u}$) for a unidirectional piezoelectric plate ($a/H = 4$) subjected to singly sinusoidal mechanical loading.

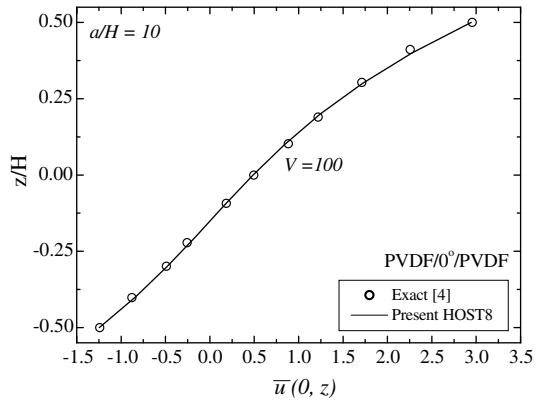

Fig. 3b. Comparison of normalized variation of in-plane displacement ($\bar{u}$) for a unidirectional piezoelectric plate ($a/H = 10$) subjected to coupled singly sinusoidal mechanical loading and electric potential ($V = 100$).

is almost zero for $V = 500$. Figs. 5a and 5b show through thickness variation of in-plane normal stress (σ_x) for $a/H = 4$; it show opposite nature of stress at top and bottom of the substrate when subjected to voltage. Normalized

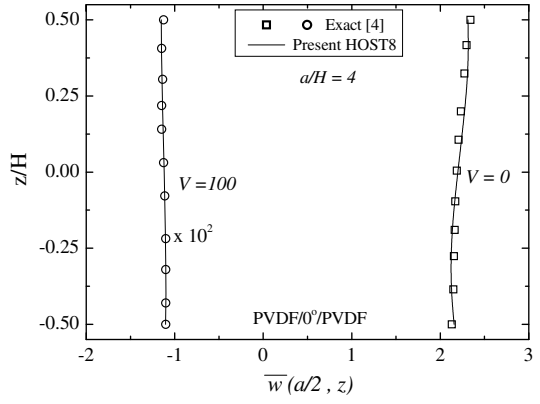

Fig. 4a. Comparison of normalized variation of transverse displacement ($\bar{w}$) for a unidirectional piezoelectric plate ($a/H = 4$) subjected to singly sinusoidal mechanical loading ($V = 0$) and coupled singly sinusoidal mechanical loading and electric potential ($V = 100$).

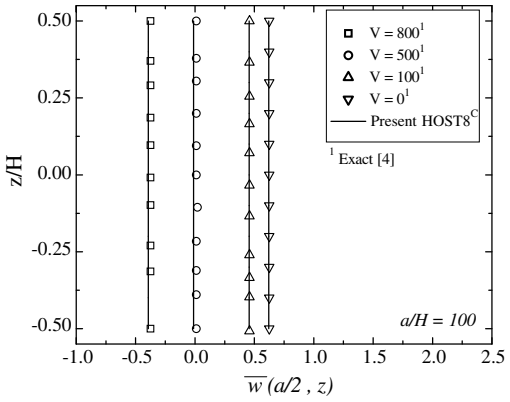

Fig. 4b. Comparison of normalized variation of transverse displacement ($\bar{w}$) for a unidirectional piezoelectric plate ($a/H = 100$) subjected coupled singly sinusoidal mechanical loading and electric potential ($V = 0$, 100, 500 and 800).

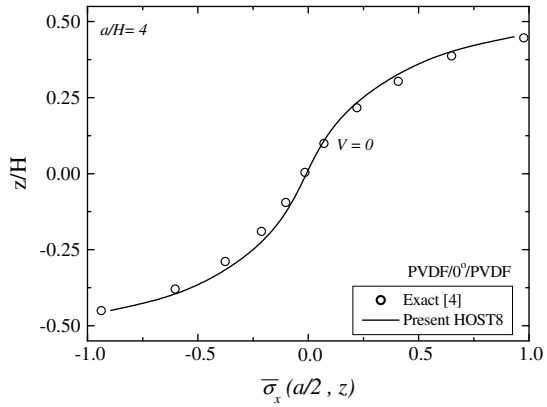

Fig. 5a. Comparison of normalized variation of in-plane normal stress ($\bar{\sigma}_x$) for a unidirectional piezoelectric plate ($a/H = 4$) subjected to singly sinusoidal mechanical loading.

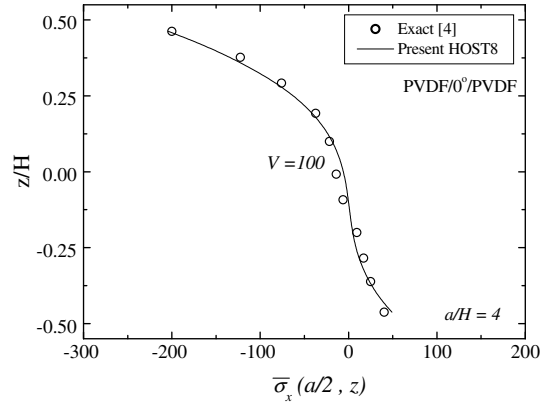

Fig. 5b. Comparison of normalized variation of in-plane normal stress ($\bar{\sigma}_x$) for a unidirectional piezoelectric plate ($a/H = 4$) subjected to coupled singly sinusoidal mechanical loading and electric potential ($V = 100$).

variation of transverse shear stress (τ_{xz}) subjected to mechanical loading is presented in Fig. 6a. The thickness of piezoelectric layer is small as compared to thickness of

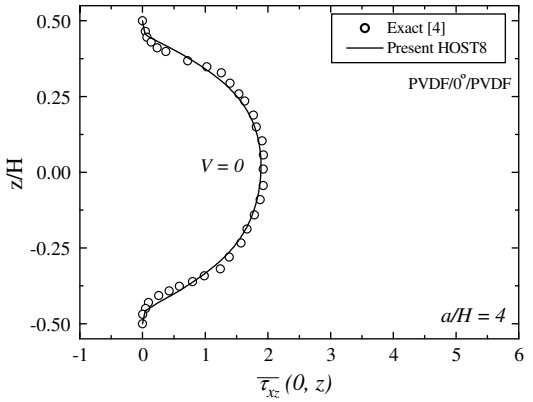

Fig. 6a. Comparison of normalized variation of transverse shear stress ($\bar{\tau}_{xz}$) for a unidirectional piezoelectric plate ($a/H = 4$) subjected to singly sinusoidal mechanical loading.

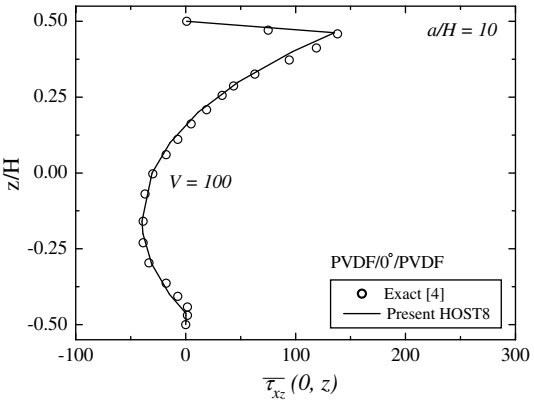

Fig. 6b. Comparison of normalized variation of transverse shear stress ($\bar{\tau}_{xz}$) for a unidirectional piezoelectric plate ($a/H = 10$) subjected to coupled singly sinusoidal mechanical loading and electric potential ($V = 100$).

elastic layer or substrate, nature of variation is not much affected when compared with elasticity solution of non-piezoelectric plate, illustrated in Fig. 2d.

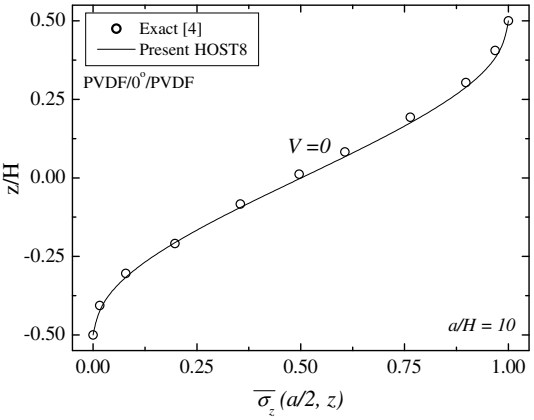

Fig. 7a. Comparison of normalized variation of transverse normal stress ($\bar{\sigma}_z$) for a unidirectional piezoelectric plate ($a/H = 10$) subjected to singly sinusoidal mechanical loading.

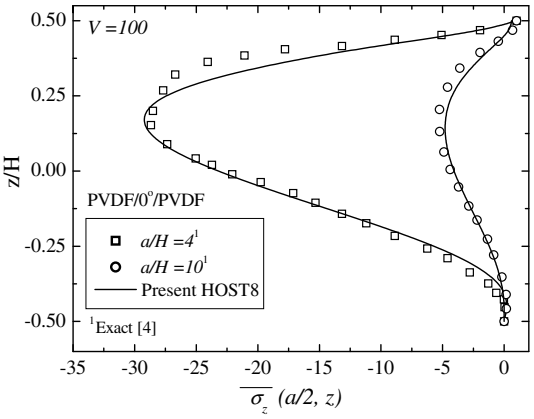

Fig. 7b. Comparison of normalized variation of transverse normal stress ($\bar{\sigma}_z$) for a unidirectional piezoelectric plate ($a/H = 4$, 10) subjected to coupled singly sinusoidal mechanical loading and electric potential ($V = 100$).

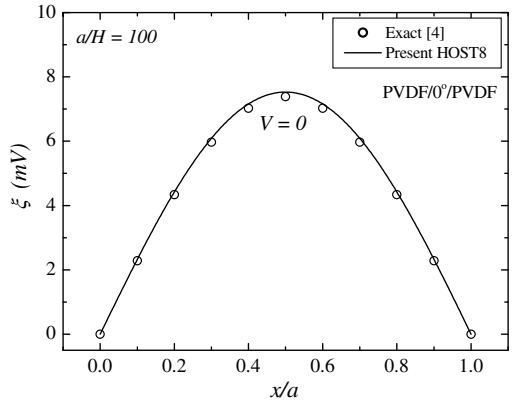

Fig. 8a. Comparison of variation of induced electric potential (ξ) along the length of the plate (x/a) for a unidirectional piezoelectric plate ($a/H = 100$) subjected to singly sinusoidal mechanical potential ($V = 0$).

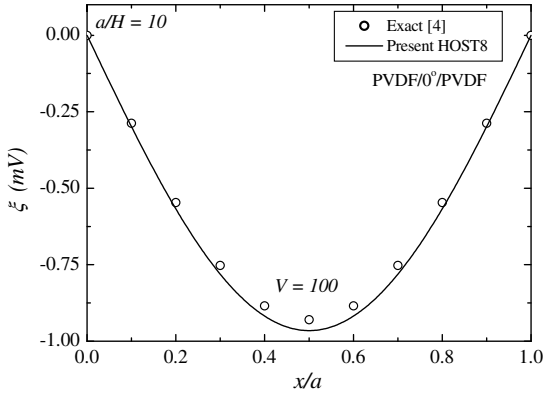

Fig. 8b. Comparison of variation of induced electric potential (ξ) along the length of the plate (x/a) for a unidirectional piezoelectric plate ($a/H = 10$) subjected to coupled singly sinusoidal mechanical loading and electric potential ($V = 100$).

Fig. 6b demonstrates transverse shear traction (τ_{xz}) at top of the substrate or at interface for $a/H = 4$. The elastic layer is subjected to heavy transverse shear stress at top interface, when subjected to electric loading; the results are in good agreement with exact solution [4].

Figs. 7a and 7b show normalized transverse normal stress (σ_z) for $a/H = 4$ and 10 for both loading conditions. Induced electric potential at the bottom of the sensor layer is shown in Figs. 8a and 8b for $a/H = 100$ displaying positive gain and for $a/H = 10$ it shows negative gain for $V = 0$ and $V = 100$, respectively.

5. Concluding remarks

Higher order shear and normal deformation theory is developed for smart laminated plates under cylindrical bending. The main objective of the analytical solution is to study the effect of electrical potential on piezoelectric plates. A total of eight degrees of freedom in the primary displacement field is assumed. Exact electric potentials in higher order terms of elastic displacement fields are obtained. The results are obtained for displacements, stresses and induced electric potential at bottom of the sensor under mechanical loading with or without application of electric potential. It is seen that present higher order theory predicts results very close to that of exact solution for smart unidirectional plates especially for transverse shear stress and induced electric potential.

References

[1] Tiersten HF. Linear piezoelectric plate vibrations. New York: Plenum Press; 1969.
[2] Mindlin RD. Forced thickness-shear and flexural vibrations of piezoelectric crystal plates. J Appl Phys 1952;23(1):83–8.
[3] Ray MC, Rao KM, Samanta B. Exact analysis of coupled electroelastic behaviour of a piezoelectric plate under cylindrical bending. Comput Struct 1992;45:667–77.
[4] Ray MC, Rao KM, Samanta B. Exact solution for static analysis of an intelligent structure under cylindrical bending. Comput Struct 1993;47:1031–42.
[5] Heyliger P, Brooks S. Exact solutions for laminated piezoelectric plates in cylindrical bending. ASME J Appl Mech 1996;63:903–10.
[6] Saravanos D, Heyliger P. Mechanics and computational models for laminated piezoelectric beams, plates and shells. ASME Appl Mech Rev 1999;52(10):305–20.
[7] Dube GP, Kapuria S, Dumir PC. Exact piezothermoelastic solution of simply-supported orthotropic flat panel in cylindrical bending. Int J Mech Sci 1996;38(11):1161–77.
[8] Shang F, Wang Z, Zhonghua L. Analysis of thermally induced cylindrical flexure of laminated plates with piezoelectric layers. Compos Part B 1997;28:185–93.
[9] Dumir PC, Kapuria S, Sengupta S. Assessment of plate theories for hybrid panel in cylindrical bending. Mech Res Commun 1998;25(3):353–60.
[10] Reissner E. The effect of transverse shear deformation on the bending of elastic plates. ASME J Appl Mech 1945;12:69–77.
[11] Mindlin RD. Influence of rotatory inertia and shear on flexural motions of isotropic, elastic plates. ASME J Appl Mech 1951;18: 31–8.
[12] Vel SS, Batra RC. Cylindrical bending of laminated plates with distributed and segmented piezoelectric actuator/sensors. AIAA J 2000;38(5):857–67.

[13] Chen WQ, Ying J, Cai JB, Ye GR. Benchmark solution of imperfect angle-ply laminated rectangular plates in cylindrical bending with surface piezoelectric layers as actuator and sensor. Comput Struct 2004;82:1773–84.
[14] Saravanos D. Mixed laminate theory and finite element for smart piezoelectric composite shell structures. AIAA J 1997;35(8):1327–33.
[15] Ballhause D, D'Ottavio M, Kroplin B, Carrera E. A unified formulation to assess multilayered theories for piezoelectric plates. Comput Struct 2005;83:1217–35.
[16] Kogl M, Bucalem ML. A family of piezoelectric MITC plate elements. Comput Struct 2005;83:1277–97.
[17] Carrera E. An improved Reissner–Mindlin type model for the electro-mechanical analysis of multilayered plates including piezo-layers. J Intell Mater Syst Struct 1997;8:232–48.
[18] Mannini A, Gaudenzi P. Multi-layer higher-order finite elements for the analysis of free-edge stresses in piezoelectric actuated laminates. Compos Struct 2003;61:271–8.
[19] Gaudenzi P, Bathe KJ. An iterative finite element procedure for the analysis of piezoelectric continua. J Intell Mater Syst Struct 1995;6(2):266–73.
[20] Roccella S, Gaudenzi P. On the formulation of a piezoelectric plate model. J Intell Mater Syst Struct 2005;16(4):285–90.
[21] Gaudenzi P. Exact higher order solutions for a simple adaptive structure. Int J Solids Struct 1998;35(26–27):3595–610.
[22] Kant T. Numerical analysis of thick plates. Comput Meth Appl Mech Eng 1982;31:1–18.
[23] Manjunatha BS, Kant T. Different numerical techniques for the estimation of multiaxial stresses in symmetric/unsymmetric composite and sandwich beams with refined theories. J Reinf Plast Compos 1993;12:2–37.
[24] Manjunatha BS, Kant T. New theories for symmetric/unsymmetric composite and sandwich beams with C0 finite elements. Compos Struct 1993;23:61–73.
[25] Kant T, Swaminathan K. Analytical solutions for the static analysis of laminated composite and sandwich plates based on a higher order refined theory. Compos Struct 2002;56:329–44.
[26] Kant T, Desai Y, Pendhari S. Stress analysis of laminates under cylindrical bending. Commun Numer Meth Eng 2008;24:15–32.
[27] Kant T, Pendhari SS, Desai YM. A novel finite-element numerical-integration model for composite laminates supported on opposite edges. J Appl Mech 2007;74:1114–24.
[28] Kant T, Pendhari SS, Desai YM. A new partial finite element model for statics of sandwich plates. J Sandwich Struct Mater 2007;9:487–520.
[29] Kant T, Pendhari SS, Desai YM. A general partial discretization methodology for interlaminar stress computation in composite laminates. Comput Model Eng Sci 2007;17:135–61.
[30] Pendhari SS. A new partial discretization technique in elastostatics with special reference to layered laminated composites and sandwiches, PhD Thesis. Bombay, India: IIT; 2006.
[31] Cady WG. Piezoelectricity. New York: McGraw-Hill; 1946.
[32] Tzou HS, Pandita S. A multi-purpose dynamic and tectile sensor for robot manipulators. J Robot Syst 1987;4:719–41.
[33] Maxwell JC. A dynamical theory of the electromagnetic field. Royal Soc Trans 1865;155:459–512.
[34] Tzou HS, Tseng CI. Distributed piezoelectric sensor/actuator design for dynamic measurement/control of distributed parameter systems: a piezoelectric finite element approach. J Sound Vibrat 1990;138:17–34.
[35] Pagano NJ. Exact solutions for composite laminates in cylindrical bending. J Compos Mater 1969;3:398–411.